Communications on Applied Nonlinear Analysis
ISSN: 1074-133X
Vol 32 No. 10s (2025)

Design and Analysis of Compact CPW-Ultra Wideband Microstrip Patch Antenna for V2X, Sub-6GHz, and other Wireless Applications

Neetu Gupta[1], Prem Pal Singh[2], Sudhir Kumar Sharma[3]

[1] Research Scholar, Department of Electronics and Communication Engineering, Jaipur National University, Jaipur, India

[2] Assistant professor, Department of Electronics and Communication Engineering, Parul University, Vadodara, Gujarat, India

[3]Head, Department of Electronics and Communication Engineering, Jaipur National University, Jaipur, India

Corresponding authors, email address: neetusinrela@gmail.com,

[2]prempal.singh38023@paruluniversity.ac.in, and [3]*sudhir.732000@gmail.com*

Article History:

Received: 12-01-2025

Revised: 15-02-2025

Accepted: 01-03-2025

Abstract: Contemporary advancements in communication systems engineering necessitate the creation of miniature antennas that provide superior performance across a wide spectrum of frequencies. In this paper, it is constructed of a small-sized (coplanar waveguide) CPW wideband microstrip antenna. This antenna is constructed of a 50Ω feed line and a circular patch with radius 5.25mm etched on the small-size FR-4 substrate of $(16 \times 13 \times 1.6)mm^3$ with relative permittivity. The proposed antenna is capable of operating from 4 GHz to 13.19 GHz frequency with a 9.19 GHz bandwidth. The proposed antenna's gain can be observed at different frequencies. This antenna is appropriate for use in C, WiMAX, WLAN, 4G LTE, 5G midband, V2X, sub 6GHz, UWB, X, and Ku band. It is simulated by using ANSYS High Frequency Structured Simulations (HFSS) software. Experimental confirmation is provided for the simulation results. To improve antenna parameters, including bandwidth and return loss, S_{11}, many types of slots are created in the ground plane

Keywords: Microstrip patch antenna, return loss, MSA, wideband, CPW, V2X.

1. Introduction

Microstrip antennas have been considered important components of all communication systems. A microstrip antenna (MSA) is a metallic conductor that transmits and receives radio waves. [1] Due to their distinctive low-profile microstrip antenna are very popular and widely used in communication systems [2]. For the increase of the bandwidth of MSA, many methods have been used. [3,4]. such as inserting multiple slots in its ground plane [5], multiple feed microstrip patch antennas methods [7], these techniques may be divided into two groups: contacting feed methods and non-contacting feed methods[24]. Contacting feed techniques, RF power is directly fed into the patch of the MSA. Examples of this method are microstrip feed and coaxial feed. In a non-contacting feed technique, the antenna patch receives its RF power indirectly by electromagnetic coupling, which carries the RF power to the patch [8]-[9]. Usually, achieving a wideband microstrip patch antenna comes at an increase of either radiation performance or size (thickness/area) [10].

The usage of corporate feeding lines, CPW-fed antenna, and microstrip patch antenna for wideband or multiband and configurable systems has been explained in several studies [2], [25], [26]. A wideband

coplanar waveguide (CPW) antenna developed for use with Wi-Fi 5 and Wi-Fi 6. The dimension of this is 20×8.7×0.4 mm^3; it is made of a double T-structure loaded with a J-shaped slot and an oval-shaped ring radiator with three concentric rings. The main improvement of this work is that only a single resonance frequency at 6.2 GHz provides a wideband operation of 34.5% (5.15- 7.29 GHz). satisfying the bandwidth requirement of Wi-F-5 (5.15-5.85 GHz) and Wi-F-6 (5.925-7.125 GHz). Its gain is around 2.25dBi, a radiation efficiency above 80%, a total efficiency above 70%, and an omnidirectional radiation pattern with a low magnitude of cross polarization throughout the bands of interest [26]. A Compact CPW-fed circular patch flexible antenna for super-wideband applications, the total size of the antenna is 24×35 mm^2, with an electrical dimension of 0.18 λ × 0.13 λ at 1.66 GHz. The flexible super-wideband antenna shows that the bandwidth ratio is 33.81:1, and the bandwidth dimension (BDR) is 7462 [6]. The antenna is lightweight, low profile, cheap, and portable. It supports a broad frequency spectrum for extended wideband communications. It is covered by industrial, scientific, and medical (ISM) bands, ultra-wideband, wireless local area network (WLAN) band, worldwide interoperability for microwave access (WiMAX) band, and various frequencies of upcoming fifth generation (5G) technology [27]. The coplanar waveguide (CPW)-fed antenna operates at a frequency range 3.04 GHz – 10.70 GHz and 15.18 GHz–18 GHz (upper Ku band) with a return loss < −10 dB and a VSWR < 2. The dimensions of this CPW-fed antenna are 47 mm×25 mm×0.135 mm; it has an average peak gain of 3.94 dBi, and it is conducive for flexible and wearable Internet of Things (IoT) applications [28].

The need for low-cost, low-volume, low-profile, planar configuration, and wide-band multifrequency planar antennas has grown as technology advances annually, with most research efforts on compact Microstrip Patch Antennas (MSAs), which meet all the requirements because of their printable circuit technology [1]. Then, various concepts and configurations have been put out to boost bandwidth and achieve multiband functionality [15]. The IEEE standard for radio waves and radar engineering defines the microwave frequency bands C, X band, and Ku-Band for use in satellite communications. Due to the various operating requirements of communication devices, there has been an increase in demand recently to discover antennas that are capable of cover multiple frequency bands, such as S-band (2–4 GHz), WiMAX (3.3–3.8 GHz), 5G mid bands (3.3–3.8 GHz, 4.4–4.9 GHz), C-band (4–8 GHz), WLAN (5.15–5.825 GHz), UWB (3.1–10.6 GHz), and X-band (8–12 GHz). It is specifically utilized for radar communication frequencies, which are approximately 8.29 GHz to 11.4 GHz. Satellite altimetry and high-resolution mapping both use the Ku band. Ku Band in particular is used to track satellites in the 12.87 GHz to 14.43 GHz range [16-21].

By 2010, the research provided the 1st set of radio standards for Vehicle to Everything (V2X) communication, V2X communication based on the IEEE802.11P technology, and is referred to as Dedicated Short-Range Communication (DSRC). This communication includes Vehicle-to-Vehicle(V2V), Vehicle-to-Network (V2N) or Vehicle-to-Infrastructure (V2I), Vehicle-to-Road Side Unit (V2R), and Vehicle-to-Pedestrian (V2P) [13].

Two important communication protocols for V2X systems are cellular-V2X (C-V2X) and dedicated short-range communications (DSRC). The primary goal of DSRC, which operates in the 5.85 GHz-5.925 GHz frequency range, is to facilitate direct communication between automobiles and other road users (or roadside units). Conversely, C-V2X allows automobiles to speak with one another via base

stations on frequencies that are licensed for use by communication companies, such as 2G, 3 G, LTE, and 5G. Furthermore, if the vehicles are outside of base-station coverage, the C-V2X standard permits direct communication via the PC5 air interface in its frequency range, which is 5.905 GHz-5.925 GHz [22,23].

Currently, 5G low-earth orbit satellite communication provides improved cellular coverage outside the 5G terrestrial coverage range, which has significant implications, especially for automated and networked cars. Compact CPW microstrip patch antenna terminals that provide both terrestrial and non-terrestrial communication are necessary for wireless automobile mass market applications [11].

In the field of automotive wireless systems, 5G and vehicle-to-everything (V2X) communications using dedicated short-range communications (DSRC) are now the most important standards underway [14]. 5G technologies provide more capacity, greater coverage, quicker connections, reduced latency, and increased dependability. Vehicle-to-Everything (V2X) communications are what we want to accomplish with these technologies. These connections not only improve road safety but also boost vehicle autonomy and safety while consuming less energy and money [29]. Numerous studies have been conducted on the integration of 5G with vehicle communication systems. Researchers these days tackle issues including virtualization, network management, cloud and edge data processing, interoperability, security, privacy, and automated and intelligent networks [12].

In this paper, the antenna is designed for a wideband frequency, its operating range is from 4 GHz to 13 GHz with a bandwidth of 9 GHz, which is appropriate for use in C, WiMAX, WLAN, 4G LTE, 5G midband, V2X, sub 6 GHz, UWB, X, and Ku band. This antenna has partial ground, and many slots are made using the etching technique, due to which the current flows uniformly in the antenna.

2. Antenna Geometry and Design

Figure 1 is the geometry of the anticipated antenna, and its fabricated antenna optical photographs are shown on the right side of Figure 1(b) and (c), which show the length and width measurements by the measuring scale.

Table 1. Dimensions of the antenna

Dimension	Value(mm)	Dimension	Value(mm)
L_1	3.25	W_1	4
L_2	0.75	W_2	2
L_3	0.9	W_3	1
L_4	3.5	W_4	4.7

In this antenna ground plane is the partial ground plane with its length and width dimensions represented in table-1, three slots are inserted in the upper side of patch and two small slots are inserted in the lower side of patch with connected 50 Ω feedline, length and width dimensions of antenna each slot represented in table-1. The Ansys HFSS 2023 R2 is used for simulation. The antenna with dimensions of 13 mm×16 mm× 1.6 mm (L×W×H) is simulated with FR-4 epoxy dielectric with

relative permittivity of 4.4. The anticipated antenna is designed at 8.5 GHz frequency with the symmetrical structure, this antenna is designed on FR-4, the substrate with thickness (h) of 1.6 mm and relative permittivity ε_r=4.4. The coplanar waveguide (CPW) is designed to be 50 ohms in order to match the characteristic impedance of transmission line.

The dimensions of a single patch element antenna were calculated by using equations (1) to (4) [30]. Here, a radiating patch of a hexagonal shape is used to configure the microstrip patch antenna (MSA); the structure has been designed to function throughout the 4 GHz to 13 GHz wideband frequency range. circular microstrip patch antenna's (CMSA) resonance frequency equation may be used to calculate the resonance frequency of a hexagonal microstrip patch antenna (HMSA) [31].

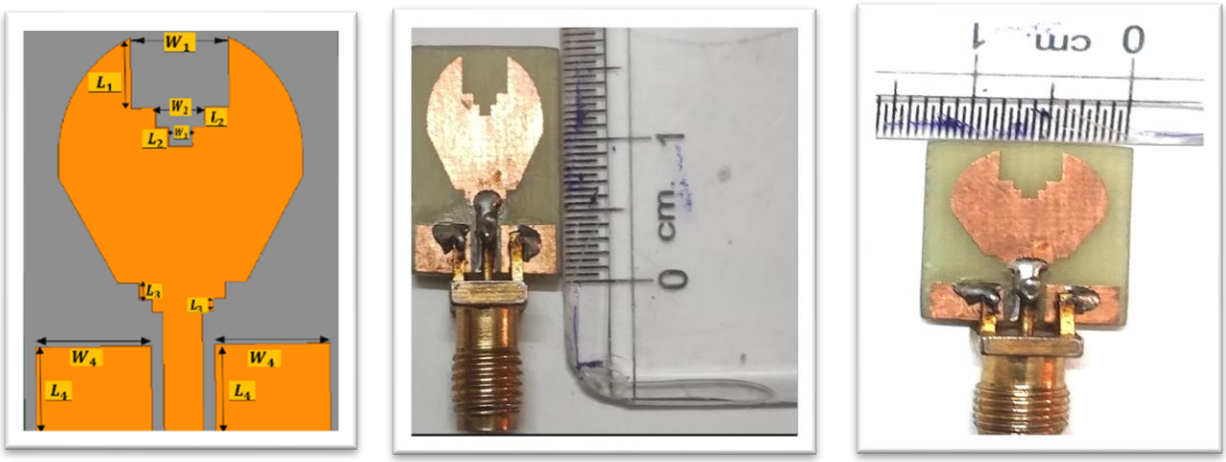

(a) **(b)** **(c)**

Figure 1 (a)Layout diagram, optical photograph of the manufactured version, (b)length measurement, (c) width measurement by the scale of the anticipated antenna

The The radius of the hexagonal patch (a_h) is obtained by

$$a_h = \frac{F}{\sqrt{\{1 + \frac{2h}{\pi\varepsilon_r F}\left[\ln\frac{\pi F}{2h} + 1.7726\right]\}}} \quad (1)$$

Where,

$$F = \frac{8.791 \times 10^9}{f_0\sqrt{\varepsilon_r}} \quad (2)$$

The side length of the hexagon patch (1) is given by,

$$\pi a_h^2 \tau = l^2 \frac{3\sqrt{3}}{2} \quad (3)$$

The height of the hexagonal patch (L) is given by

$$L = \sqrt{3}a_h \quad (4)$$

2.1 Design Evolution

Figure 1 shows the layout diagram of a patch and the layout of the partial ground plane, with dimensions of the ground plane is 12 mm×3.5 mm; the ground is modified with a slot 2.6 mm×4 mm. The patch is constructed by introducing several shapes of slots. The patch layout diagram shown in Figure 2(a), many slots in the patch for modification. It provides perfect impedance matching and proper radiation for making this slot iteration design technique used. On the upper side, three rectangular slots are introduced, 4 mm×3.5 mm, 2 mm×0.75 mm, and 0.9 mm×0.75 mm receptively.

Figure 2 illustrates the iterative design technique that was applied to create the antenna. For antenna designing, four iteration techniques are used to introduce slots in the patch, which helps to provide better performance. This process is shown in Figure 3. To design this antenna, many shapes and several rectangular slots have been introduced in the upper side, bottom side, two rectangular strips are horizontally connected with the dimensions 3.7 mm×0.7 mm and 2.5 mm×0.5 mm with feedline, and partial ground planes. Figure 3 represents the steps involved in making an anticipated antenna. Several slots are used for making a slot in the patch iteration-1 to iteration-4 sequence as follows: In iteration-1, two circles (in this, we used a circle to make hexagons, just put a value n=6) and some rectangles are used to make a patch and excited with a microstrip line of length L_f and width W_f. After this, in iteration 2, a rectangle slot 4 mm×3.25 mm is etched in the upper side of the patch. In iteration 3 with dimension 2 mm ×0.75 mm rectangle slot is etched in upper side of patch and just below the upper slot introduced by iteration 3 and finally in iteration 4 a small size rectangle with dimension 1 mm×0.75 mm is created by etching of patch it is also in upper side of patch and just below upper two slot by created iteration 2 and 3 all upper slot are unite to each other they provides good impedance matching and it helps to convert the antenna as a CPW wideband antenna, we obtain the wideband frequency 4 GHz to 13 GHz.

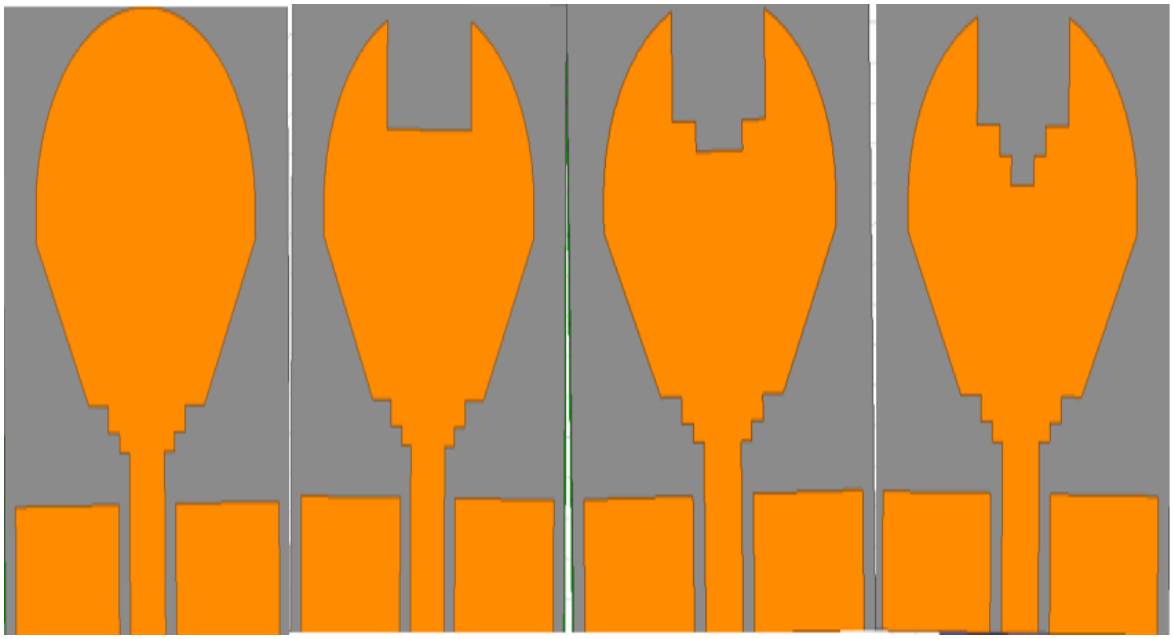

Iteration-1 **Iteration-2** **Iteration -3** **Iteration-4(anticipated antenna)**

Figure 2. Iteration technique for anticipating the antenna

The antenna that operates wideband frequencies shown in Table 2 is the outcome of the modification performed in Iteration 4. In this anticipated CPW microstrip wideband patch antenna ground and patch are on the same side, and its opposite side metal is not used. FR4-Epoxy dielectric material is used for the substrate; it's a dielectric constant $\varepsilon_r = 4.4$ and its thickness is 1.6 mm. Several shapes of slots are introduced on the patch, and finally the proposed antenna is finalized: simulated return loss parameter operating frequency from 4 GHz to 13 GHz. This antenna is compact in size, it covers C, WiMAX, WLAN, 4G LTE, 5G midband, V2X, sub 6GHz, UWB, X, and Ku band.

We can see that in Figure 3; in each iteration bandwidth patterns of the reflection coefficient are very similar to each other. Overall bandwidth responses are below the 10dB line despite a few minor variations in frequency location. The simulation result of the final iteration applied in the anticipated antenna, measured dB (S (1:1)) wide bandwidth curves from 4 GHz to 13 GHz at the operating frequency 8.5 GHz, it's a bandwidth is 9 GHz.

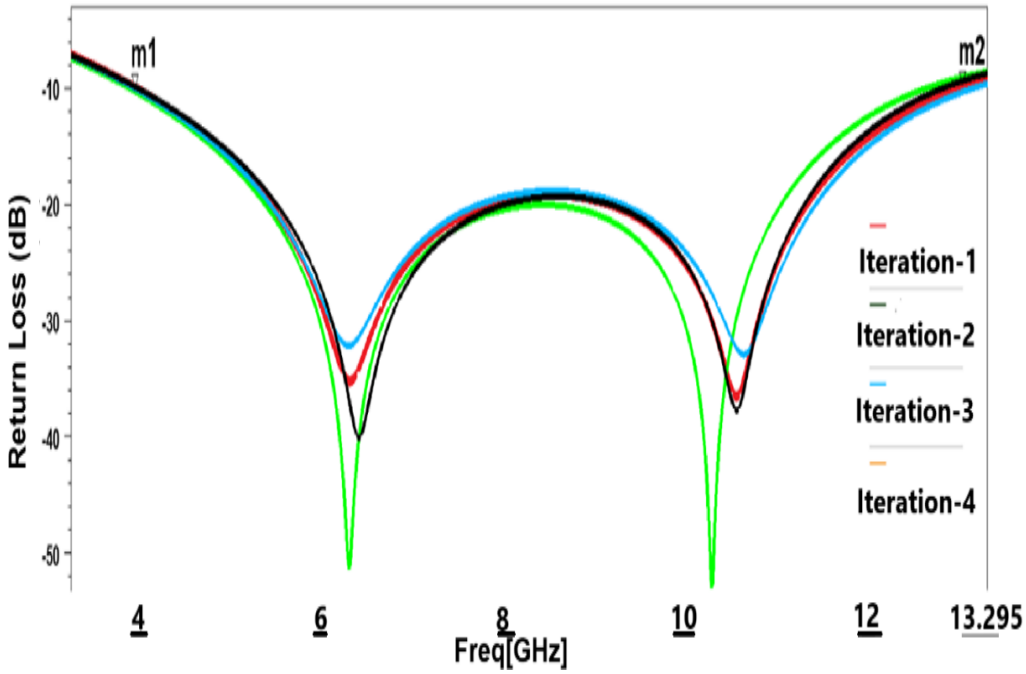

Figure 3. Reflection coefficient of all iterations

Table 2. Operating frequency ranges for four iterations

Iteration Number	**Frequency Band**	**Iteration Number**	**Frequency Band**
Iteration -1	4 GHz - 12.5 GHz	Iteration -3	4 GHz - 12.7 GHz
Iteration -2	3.9 GHz - 13.13 GHz	Iteration -4	3.9 GHz -13.03 GHz

Figure 4 shows the responses of VSWR of all iteration techniques; each response of VSWR is slightly different from the others. Finally, at the last iteration, we got the VSWR minimum value is 1.03 and maximum is 1.88, which ensures good impedance matching.

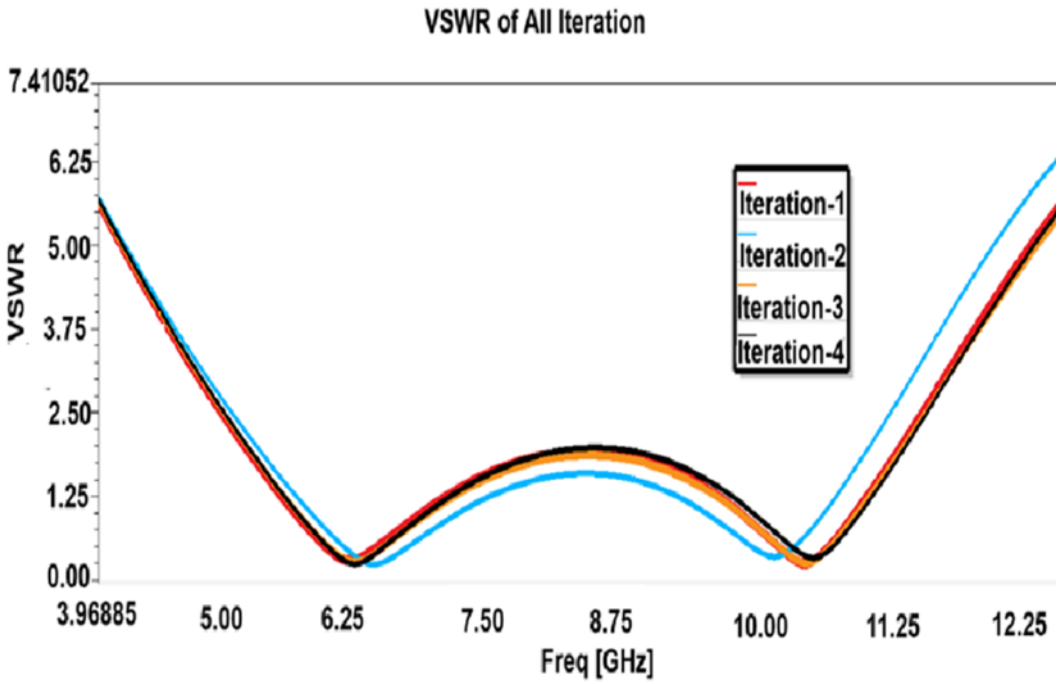

Figure 4. VSWR of each iteration

2.2 Surface Current Distribution

Figure 5 shows the current distribution of the designed antenna at operating frequencies 8.5 GHz, 5 GHz, and 6.38 GHz. We can see in the figure maximum current is distributed at the bottom side of the patch. It can be observed that the current is uniformly distributed at the lower side of the antenna.

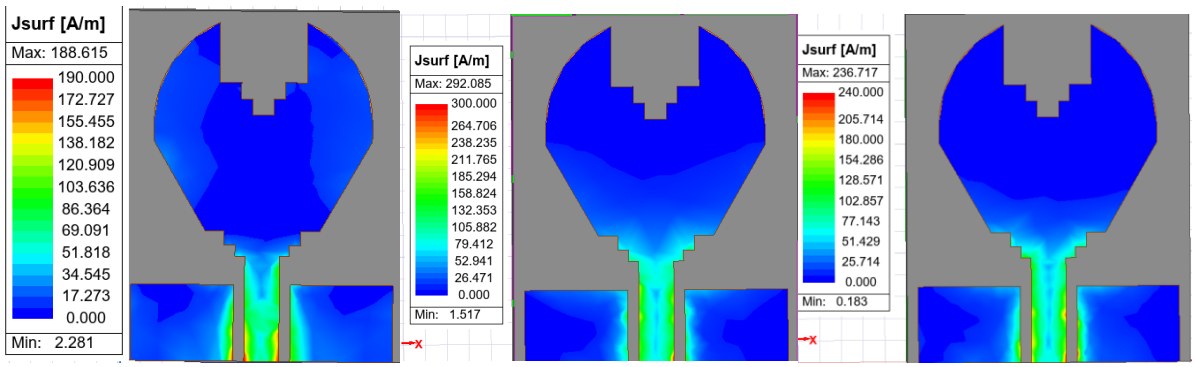

(a) **(b)** **(c)**

Figure 5. Surface current distribution. (a) 8.5 GHz (b) 5 GHz (c) 6.38 GHz

2.3 Parametric Analysis

The proposed antenna consists of three rectangular-shaped slots on the upper side of the patch and two rectangular strips parallelly connected between the bottom side of the patch and the feedline. HFSS by ANSYS software is used for the parametric analysis and optimization of the proposed antenna, which is a commercial 3D electromagnetic software. In this section, we have changed the value of L_1 and W_1 analyze the effect caused by it and investigated the variation of W_4 in the ground. It is important to note that all the dimensions of the antenna are kept fixed during the optimization of a particular parameter. The parametric analysis of the proposed antenna is as follows:

2.3.1 Variation of Length L_1

2.3.2 Variation of Width W_1

2.3.3 Variation of Width W_4

2.3.1 Variation of Length L_1

We can see that in Figure 6(a) L_1 is equal to 3.25 is the original length of the patch, for the parametric analysis L_1 is varies with the dimensions of 1.25, 4.75mm, and 5.5mm. Due to this variation, it influences the frequency band and return loss, here, it reduces the frequency band slightly. There have also been changes in return loss due to varying the length L_1We can see that the value of return loss is decreasing in Figure 9(a). Figure 6 represents the layout diagram due to the variation in length L_1.

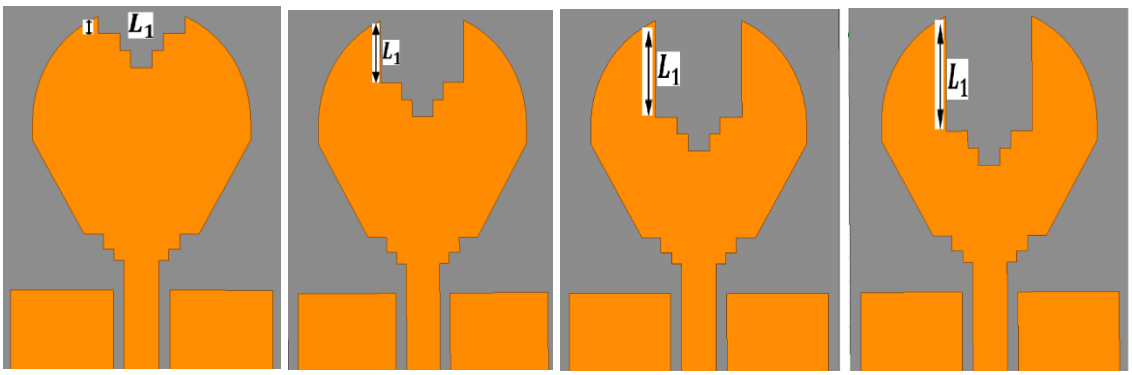

(a) (b) (c) (d)

Figure 6. Variation of length L_1 (a)1.25 mm(b) 3.25 mm (c)4.75 mm (d) 5.5 mm

2.3.2Variation of Width W_1

In Figure 9(b), we can see the change in frequency due to the variation of width W_1in the proposed antenna. If the width is 4mm (original length of the patch) W_1,We obtain the frequency band 4 GHz to 13 GHz and return loss -48 dB, but we change the value of W_1 4 mm to 6 mm, causing the return loss to be reduced to 32 dB. After this, we do more variation in width, take two different values, 3 mm and 1mm, and analyze that there is some change in the frequency band is decreasing. In Figure 7 shows the layout due to the variation of width W_1.

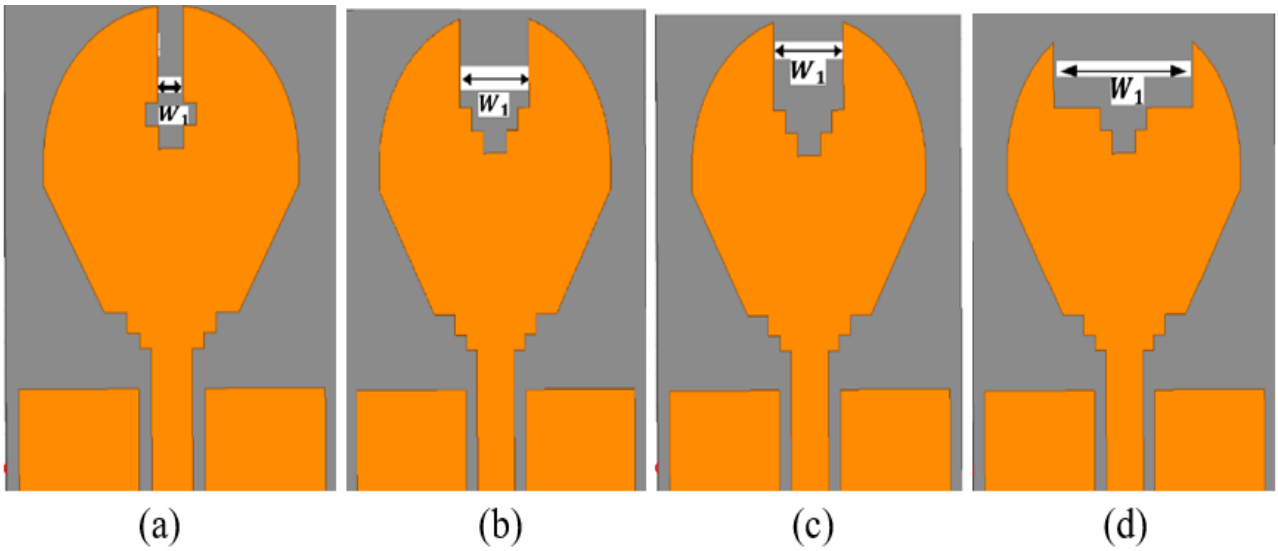

Figure 7. Variation of width w_1 (a) 1mm (b) 3mm (c) 4mm (d) 6mm

2.3.3 Variation of Width W_4

Figure 9(c) shows the return loss plot with different dimensions of width W_4 of ground. From the graph shown above, it is clear that as the width W_4 Varying the return loss plot shows poor results. Consequently,4.4mm is the ideal ground width since anything that changes leads to poor return loss, and due to W_4 variation affects the frequency band and reduces it. in this section, we have analyzed that when the length L_1, width W_1 and W_4 are varied, and they directly affect the bandwidth.

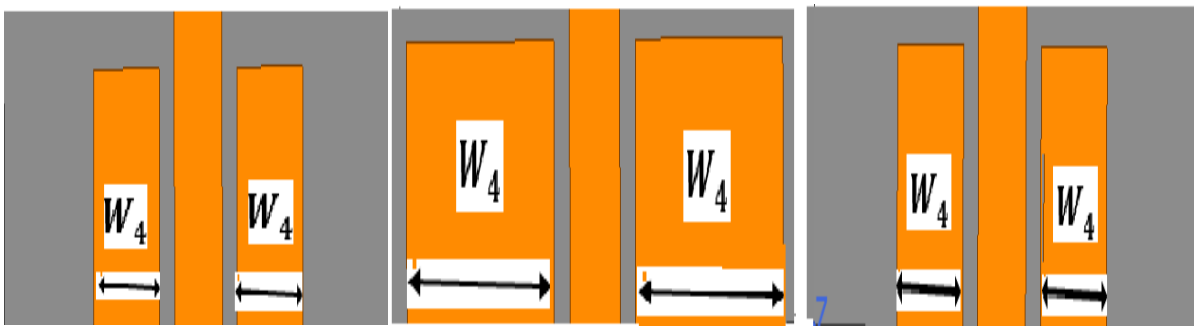

Figure 8. Variation of width w_4(a) 2.2mm(b) 3.525mm (c) 4.7mm

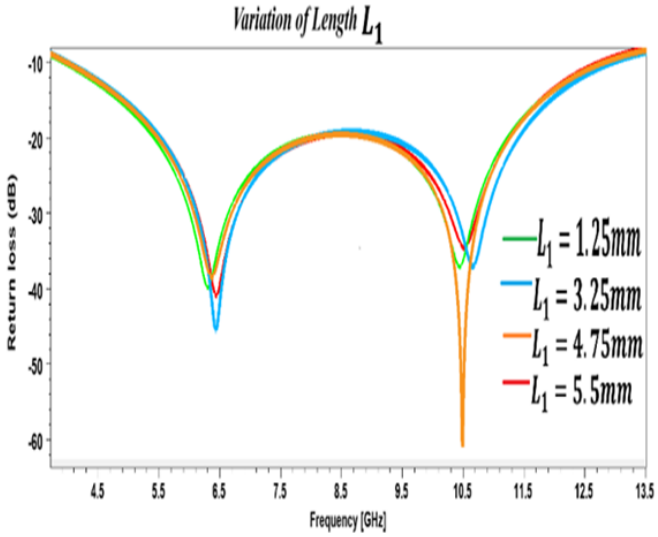

(a)

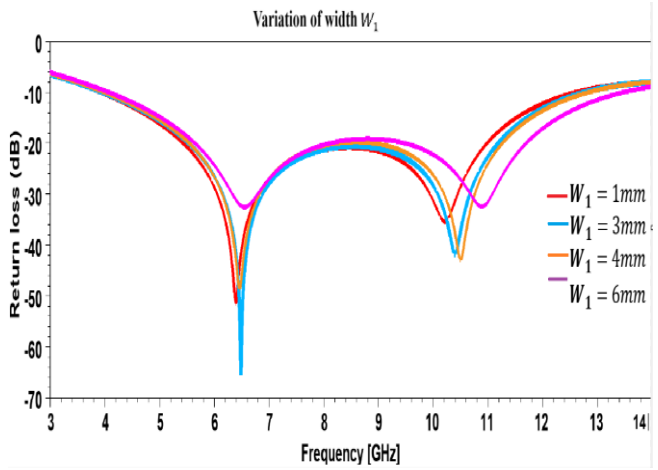

(b)

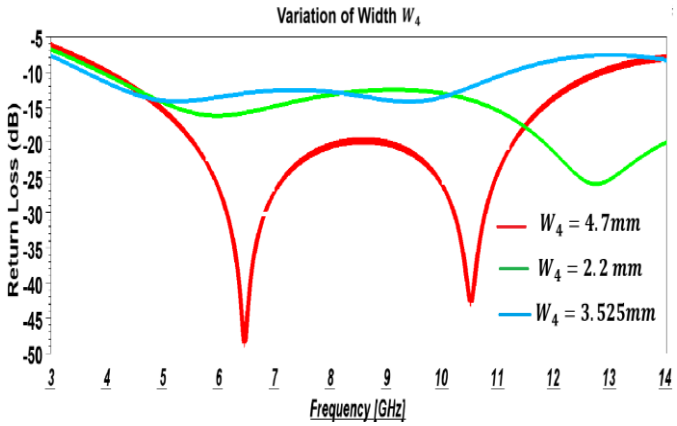

(c)

Figure 9. Variation of (a) length L_1 (b) width W_1 in the patch and (c) width in the ground W_4

3. Results and Discussions

The prototype is fabricated to validate performance, and the result of the simulated antenna. A 1.6 mm thick FR-4 substrate with a dielectric constant (ε_r) of 4.4 is used. A commercially available 50 Ω SMA connection powers the antenna, which is small. HFSS software is used to test the reflection coefficients. Antenna performance is investigated and analyzed in terms of like reflection coefficients, gain, and radiation pattern. Simulated results for reflection coefficients of the fabricated antenna shown in Figure 9, we have got a wide bandwidth and maximum gain occurred at 4.30dBi from the simulated results can be observed. The overview of operating frequencies and simulated return loss (S11) values, and gain is presented in Table 3

Table 3. Summarized result at different frequencies

Operating Frequency (GHz)	Return Loss (S11) (dB)	Gain(dBi)
7.5GHz	-37.38	1.06
8.5GHz	-43.67	2.04
12GHz	-35.35	3.91
13GHz	-35.86	4.30

Observed the impedance bandwidth for S11 ≤ -10dB is 9 GHz, its operating frequency is from 4 GHz to 13 GHz, and the maximum return loss obtained is -45.42 dB, which is a function of frequency. From the reflection coefficient values achieved, we can say that the antenna has a better impedance matching along with all the resonating frequencies. Figure 11 shows the 3D polar plot of the radiating patch. This diagram represents the gain of the antenna, we can observe that this polar plot shows the total gain of an antenna in different directions, color-coded to represent the gain values in decibels (dB). The color bar on the left represents the gain values in decibels, ranging from -25 dB (blue) to +5 dB (red). Red areas indicate regions of high gain (up to 5 dB), while blue areas represent regions of low gain (down to -25 dB). In 3D Radiation Pattern at 7.5 GHz is shown in Figure 11(a). The shape depicted is almost spherical, meaning that the antenna radiates nearly uniformly in all directions, but with variations in intensity. Green and yellow areas near the center represent regions of moderate gain (between -5 and -15 dB). The center of the sphere (blue region) shows the lowest gain (about -23 dB), indicating weaker radiation in this direction. In 11(a) figure top right shows the gain value, the annotation dB (Gain Total) = 1.05977E+00 shows that the total gain of the antenna is around 1.06 dB, which is a positive value, suggesting that the antenna radiates more energy than an isotropic radiator in some directions. The coordinate axes (X, Y, Z) in the lower-left corner indicate the orientation of the radiation pattern relative to the antenna's position. This helps in identifying which directions correspond to the different regions of gain. The radiation pattern is nearly omnidirectional, with most regions having relatively uniform gain (as suggested by the red outer regions). The gain variation across the pattern shows that the antenna is not perfectly isotropic but radiates more energy in some directions compared to others. The central dip (blue region) indicates a direction of low radiation or null in the gain, where the antenna emits much less energy compared to other directions. This 3D

radiation plot shows that the antenna radiates energy almost uniformly in most directions, with some variations in gain. The red areas indicate stronger radiation, while the blue areas correspond to weaker radiation. This pattern is characteristic of an antenna designed for near-omnidirectional coverage but with some directionality.

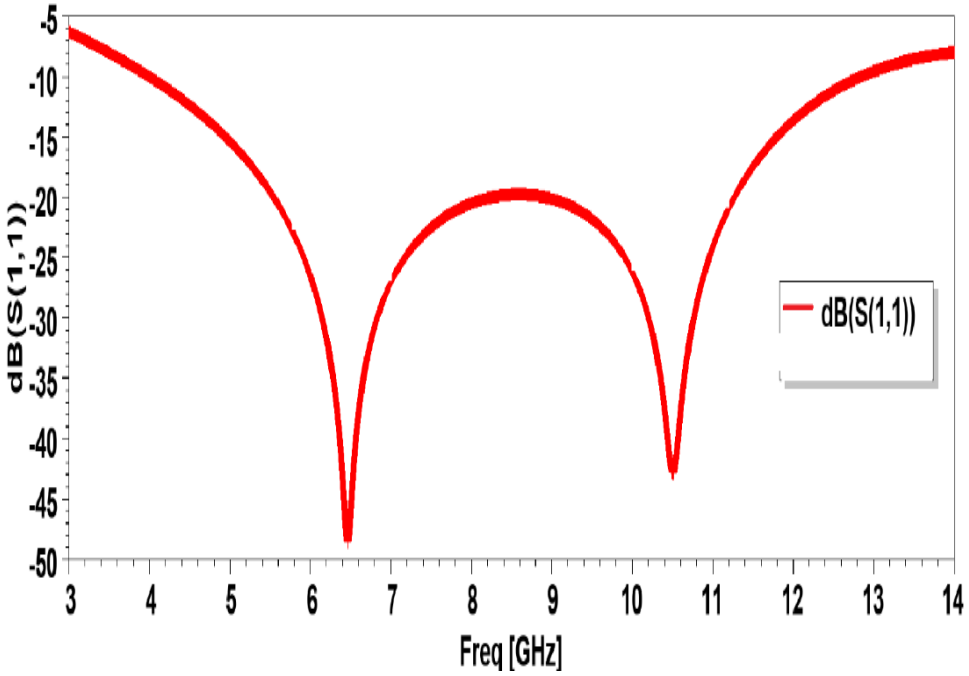

Figure 10. Return loss (S11) of the proposed antenna

Figure 11(b) represents the gain total of a proposed antenna in decibels (dB) over a spherical surface at 8.5 GHz. The colors range from red (highest gain, 2.04 dB) to blue (lowest gain, -21.89 dB). This shows how the gain varies in different directions. The sphere's colors correspond to the gain values, with red indicating the highest gain areas and blue the lowest. The value "2.03848E+00" at the top right indicates a specific gain measurement. This visualization helps in understanding the directional performance of the antenna, showing where it radiates most effectively.

In Figure 11(c), this image shows a 3D radiation pattern plot for an antenna at 12 GHz, illustrating how the signal strength varies in different directions. Color-Coded Strength: The colors range from red (strongest signal, 5 dB) to green (weakest signal, -40 dB). Intermediate strengths are shown in yellow and light green. This line might indicate a plane of symmetry or a specific measurement direction. The text in the figure represents the "3.90560E+00 dB (Gain Total)", a specific gain measurement at a point on the plot. This visualization helps in understanding the directional performance of the antenna, showing where it radiates most effectively.

Figure 11(d) represents a 3D radiation pattern plot for an antenna at 13 GHz, showing how the signal strength varies in different directions. The scale on the left ranges from -41.85 dB (blue) to 4.30 dB (red). This indicates the signal strength, with red showing the strongest signals and blue the weakest. The sphere's colors transition smoothly from red to the highest gain areas to blue at the lowest, passing

through intermediate colors like yellow and green. The plot is a 3D sphere, which helps visualize how the antenna radiates signals in all directions. The text “Max: 4.30” and “dBi (Gain Total) 4.30138E+00” at the top right corner indicate the maximum gain measured in decibels. This value represents the overall effectiveness of the antenna in converting input power into radio waves in a specific direction. We obtain the simulated gain of the antenna is 1.06 dBi at 7.5 GHz, 2.04 dBi at 8.5 GHz, 3.91 dBi at 12 GHz, and 4.3 dBi at 13 GHz frequency.

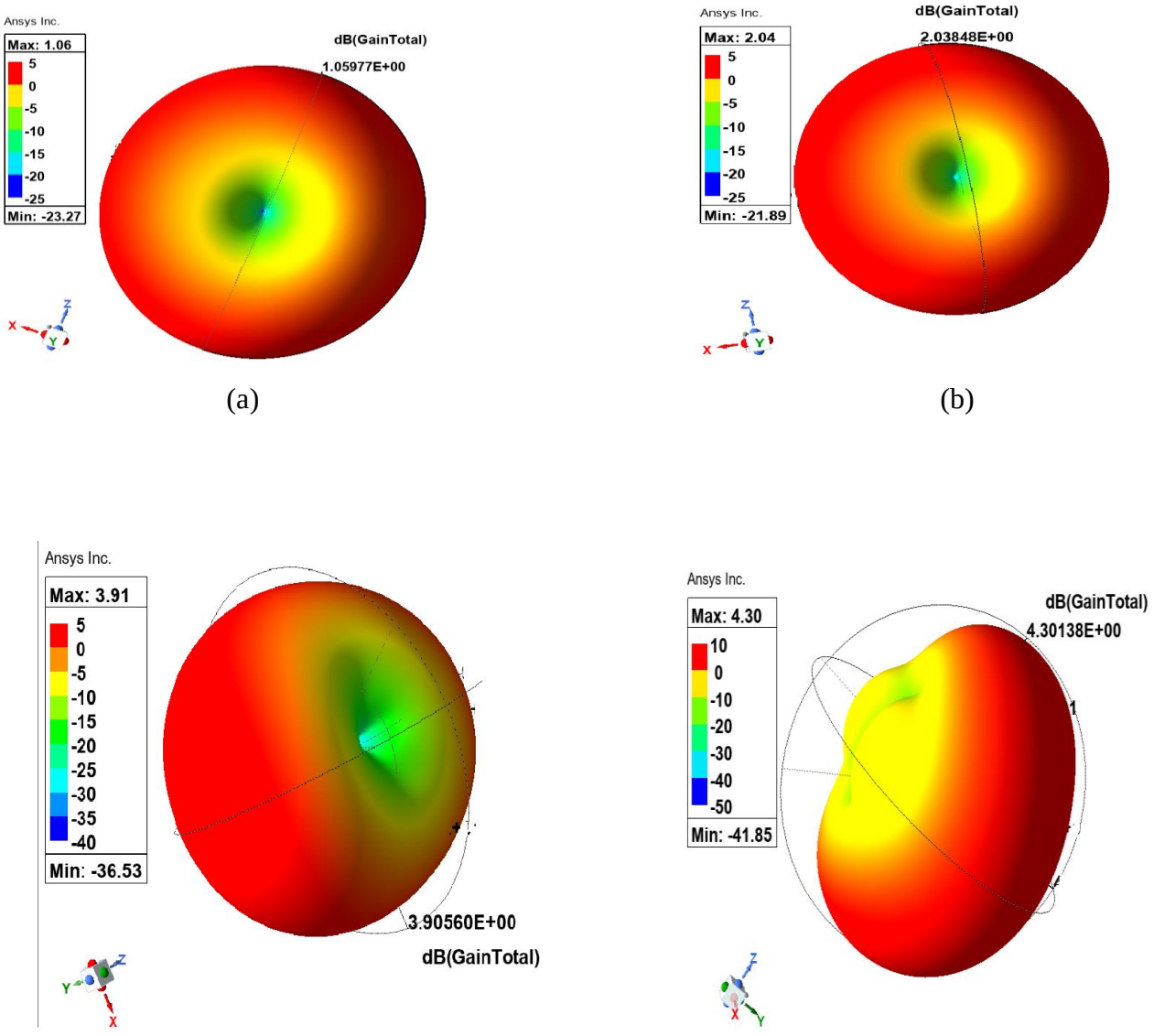

Figure 11. Gain of the antenna (a) 7.5 GHz (b) 8.5 GHz (c) 12 GHz (d) 13 GHz

Figure 12 shows the simulated radiation pattern, which radiates as a ‘figure of eight (also known as a dipole-like pattern or "bi-lobed" pattern) in both the elevation plane and the azimuth plane. Radiation pattern at 7.5 GHz.

This figure 12 (a) is a polar plot showing the antenna gain pattern (in decibels, dB) at a frequency of 7.5 GHz in figure shows two different first one is azimuth angle and other one is elevation angle orientations of the antenna, right side plot are two different curves (green and red), indicating different radiation behaviors in this plane. Theta (elevation angle) for two Phi angles. The green plot represents the antenna's gain pattern for a constant elevation angle Phi = 90. The shape of the pattern resembles a "figure of eight" or a clover-leaf pattern, indicating two major lobes of radiation with nulls (minimal radiation) between them. The maximum gain is around 4 dB, and there are clear nulls around ±90°. Where strong radiation occurs in two opposite directions (forward and backward lobes), with nulls orthogonal to the main lobe direction. Red plot (Phi = 0°). The gain is much lower compared to the green curve. The maximum gain is around -18 dB, which is relatively low. The pattern is irregular, with multiple lobes, indicating that the antenna has weaker radiation in this plane.

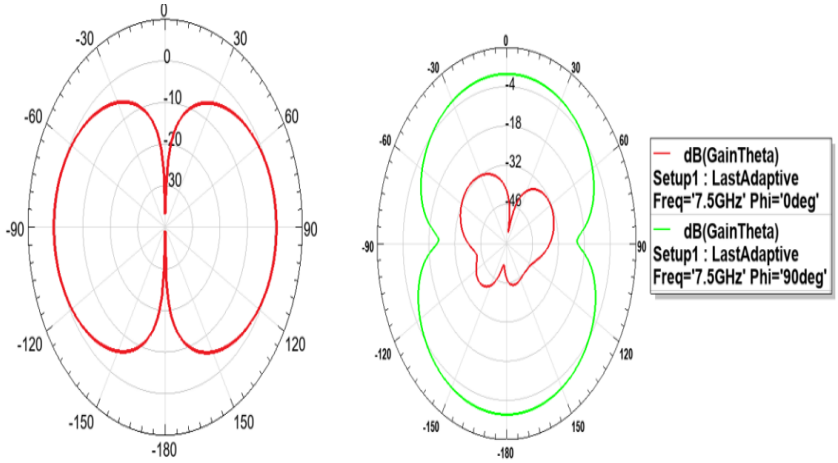

(a)

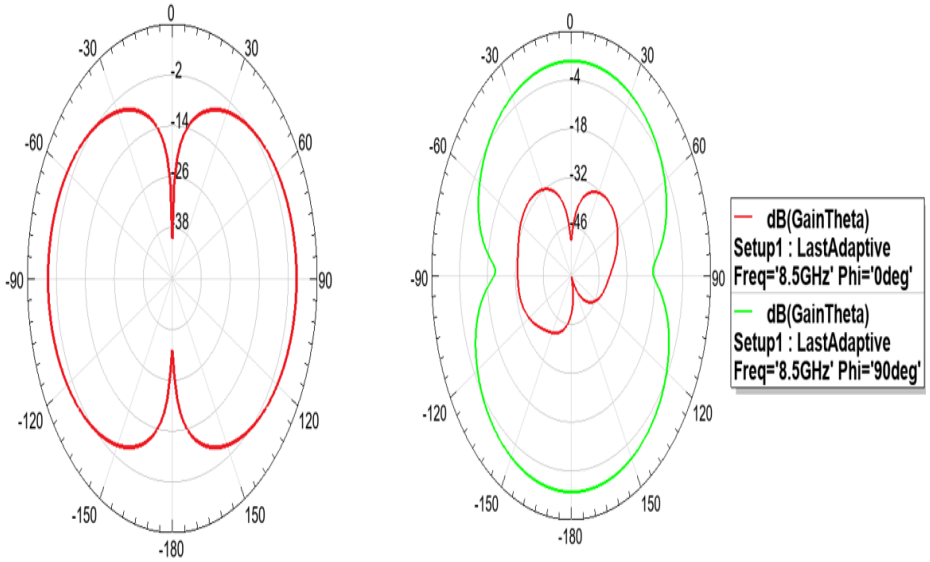

(b)

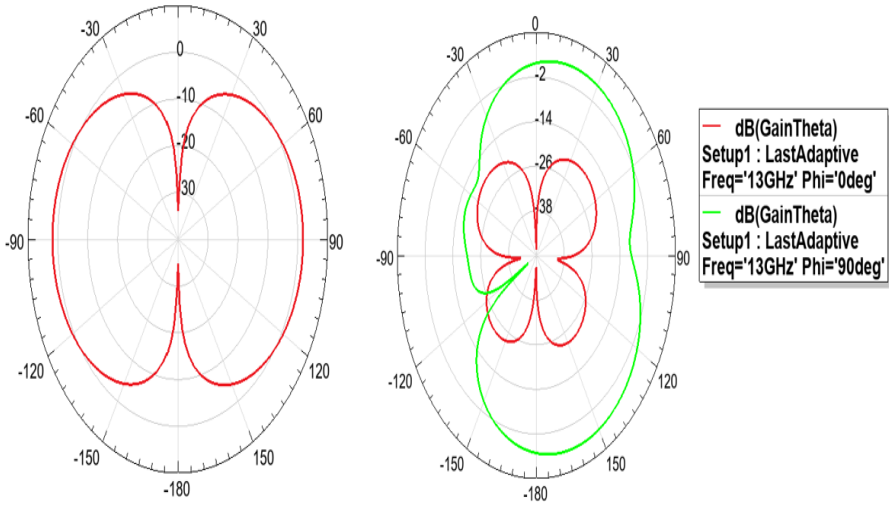

(c)

Figure 12. Radiation pattern of gain (a)7.5 GHz (b)8.5 GHz (c)13 GHz

Left side plot shows how the antenna radiates in the plane where Phi = 0°, its azimuth figure shows a typical dipole or bi-directional antenna radiation pattern, where the antenna radiates strongly in two opposite directions (±90° and ±270°) at maximum gain occurs (~30 dB), with no radiation at 0° and 180°.The pattern suggests a broadside radiation behavior, meaning the antenna radiates strongest in the horizontal plane (perpendicular to its main axis).

Figure 12 (b) shows the radiation pattern at 8.5 GHz, this polar plot displays the radiation pattern of an antenna at 8.5 GHz, this polar plot represents the gain (dB) vs. Theta (elevation angle) at a frequency of 8.5 GHz, for two different azimuthal angles (Phi = 0° and Phi = 90°). It helps in understanding how the antenna radiates energy in different planes. Phi = 0° (Red Plot) and Phi = 90° (Green Plot), the green curve represents the antenna's radiation pattern for Phi = 90°. The shape is a figure-eight or bi-lobed pattern, with two main lobes that are opposite each other. The gain in the main lobes is around -4 dB, while the nulls (points where the radiation is weakest) go down to around -46 dB. This indicates that the antenna radiates strongly in the direction of the lobes but has very weak radiation perpendicular to these lobes. This pattern is directional, meaning the antenna primarily radiates energy in two directions. Maximum radiation occurs at 0 and 180º, and minimum radiation occurs at ±90º. Red Plot (Phi = 0°), the red curve represents the antenna’s radiation pattern for Phi = 0°. The pattern is a figure-eight; in the antenna radiates bidirectional in this plane. The gain is around -48 dB, indicating slightly reduced radiation in both directions in this plane compared to the Phi =90° pattern. Maximum radiation occurs in the ±90º and minimum radiation occurs at 0 and 180º.

The left red plot indicates a specific Phi-plane measurement, with strong radiation in two opposite directions and minimal radiation in perpendicular directions. This is typical of antennas that radiate in a dipole-like manner. Maximum gain occurs ~38 dB at ±90° (broadside direction) and minimum gain (nulls) at 0° and 180° (end fire direction). This means the antenna radiates very little energy along its axis.

Figure 12. (c) shows the radiation pattern at 13 GHz, this right polar plot shows the antenna radiation pattern at 13 GHz for two different elevation angles: Phi = 0° and Phi = 90°. Here's the analysis: Red Plot (Phi = 0°), the red curve represents the radiation pattern for Phi = 0°. It has a four-lobed pattern, which is more complex than the typical figure-eight seen in previous plots. This indicates that the antenna radiates in four distinct directions, rather than two. The gain values in the lobes reach about -2 dB, meaning that these are the directions where the antenna radiates most strongly. The nulls (points where the radiation drops significantly) go down to about -38 dB, indicating very weak or no radiation in certain directions between the lobes. This type of pattern suggests that the antenna is more directionally complex and radiates in multiple distinct directions for this particular plane. Green Plot (Phi = 90°), the green curve represents the radiation pattern for Phi = 90°. It shows a more circular or elliptical pattern, indicating more uniform radiation in this plane. The gain is around -2 dB, and the pattern does not have deep nulls like the red curve. In the plane at Phi = 90°, the antenna radiates fairly evenly in all directions, with no significant directional preference. The red plot for Phi = 0° shows a complex directional pattern with four main lobes, indicating that the antenna radiates strongly in four specific directions. The deep nulls between the lobes suggest minimal radiation in other directions. The green plot for Phi = 90° shows a more uniform radiation pattern, meaning the antenna radiates almost equally in all directions in this plane. Phi = 0° (red curve): A four-lobed pattern, where the antenna radiates in four distinct directions with deep nulls in between, indicating strong directionality. Phi = 90° (green curve): A more uniform elliptical radiation pattern, showing that the antenna radiates evenly in all directions in this plane. This plot illustrates the antenna's varying radiation characteristics at different azimuthal angles, highlighting a more complex radiation behavior at 13 GHz compared to previous frequencies. The left plot shows that the bidirectional radiation occurs in the ±90º and minimum radiation (null) occurs at the 0º and 180º means no radiation occurs in these directions. Maximum gain occurs at this frequency, ~30 dB.

A brief overview of the literature survey on the many types of CPW wideband antennas developed in recent years is given in Table 4. The wideband antennas are designed to operate at frequencies 4 GHz to 13 GHz, and their bandwidth is 9 GHz. Its bandwidth is maximum compared to another wideband antennas. Antenna can achieve better performance with smaller dimensions in terms of bandwidth and gain. From the comparison, it can be observed that the achieved results of this antenna are designed much better than the other designed antennas, with the attributes of smaller size, lower cost, and easy fabrication, providing sufficient bandwidth. The proposed antenna has a suitable gain, other than this.

4. Conclusion

With its ability to operate in the 4 GHz–13.19 GHz range, the proposed compact CPW-fed UWB antenna (16×13) mm^2 shows great promise for next-generation wireless communication systems. It is ideal for sub-6 GHz, 5G, V2X communication, IoT, and biomedical telemetry because of its broad impedance bandwidth, low-profile design, and planar structure. Gain augmentation using metamaterials, integration with MIMO systems for enhanced spatial diversity, and frequency reconfigurability via tenable components like varactors or PIN diodes might be the main areas of future development. The antenna's suitability for radar sensing (SAR, GPR), mm Wave transition, and cognitive radio networks can also be investigated. The antenna may get higher spectral efficiency and dynamic spectrum utilization by utilizing beamforming methods and AI-driven adaptive tuning.

Additional improvement might make this ultra-wideband CPW antenna an essential part of high-data-rate, low-latency, and energy-efficient communication networks, meeting the demands of future 5G, 6G, and beyond technologies.

Declaration Statement

After aggregating input from all authors, I must verify the accuracy of the following information as the article's author.

- Conflicts of Interest/ Competing Interests: Based on my understanding, this article has no conflicts of interest.
- Funding Support: This article has not been funded by any organizations or agencies. This independence ensures that the research is conducted with objectivity and without any external influence.
- Ethical Approval and Consent to Participate: The content of this article does not necessitate ethical approval or consent to participate with supporting documentation.
- Data Access Statement and Material Availability: The adequate resources of this article are publicly accessible.
- Authors Contributions: The authorship of this article contributed equally to all participating individuals.

Notation

In this paper, the symbols listed below are employed.

Alphabet

$\boldsymbol{L_1}$	= Length of the slot 1	mm
$\boldsymbol{L_2}$	= Length of the slot 2	mm
$\boldsymbol{L_3}$	= Length of the slot 3	mm
$\boldsymbol{L_4}$	= Length of the ground	mm
$\boldsymbol{L_f}$	= Length of the feedline	mm
$\boldsymbol{W_f}$	= width of the feedline	mm
$\boldsymbol{W_1}$	= Width of the slot 1	mm
$\boldsymbol{W_2}$	= Width of the slot 2	mm
$\boldsymbol{W_3}$	= Width of the slot 3	mm
$\boldsymbol{W_4}$	= Width of the ground	mm
dB	= Decibel	
S(1:1)	= Return loss	db
VSWR	= Voltage standing wave ratio	
h	= Thickness	mm
CPW	= Coplanar Waveguide	
MSA	= Microstrip Patch Antenna	
CMSA	= Circular Microstrip Patch Antenna	

HMSA	= Hexagonal Microstrip Patch Antenna	
VNA	= Vector Network Analyzer	
f	= Frequency	GHz

Symbol

$\boldsymbol{\varepsilon_r}$	= Relative Permittivity
Ω	= Ohm
$\boldsymbol{a_h}$	= Radius of Hexagonal Patch
~	= Approximately

References

[1] Werfelli, Houda, Tayari, Khaoula, Chaoui, Mondher, Lahiani, Mongi, & Ghariani, Hamadi. "Design of Rectangular Microstrip Patch Antenna." 2016 2nd International Conference on Advanced Technologies for Signal and Image Processing (ATSIP), pp. 798–803, 2016. DOI: 10.1109/ATSIP.2016.7523166.

[2] Zhang, Yongjian, and Yue Li. "Wideband Microstrip Antenna in Small Volume Without Using Fundamental Mode." Electromagnetic Science, vol. 1, no. 2, 2023, article no. 0020073. DOI: 10.23919/emsci.2023.0007.

[3] Abdelaziz, Abdelmonem. "Bandwidth Enhancement of Microstrip Antenna." Progress In Electromagnetics Research, vol. 63, 2006, pp. 311–317. DOI: 10.2528/PIER06051201.

[4] Akinola, Segun, Iddi Hashimu, and Ghanshyam Singh. "Gain and Bandwidth Enhancement Techniques of Microstrip Antenna: A Technical Review." Proceedings of the 2019 International Conference on Computational Intelligence and Knowledge Economy (ICCIKE), IEEE, 2019, pp. 175–180. DOI: 10.1109/ICCIKE47802.2019.9004278.

[5] Al-Ahmadi, Ahmad, and Yahya S. H. Khraisat. "Bandwidth Enhancement of Microstrip Patch Antenna." Applied Physics Research, vol. 11, no. 1, 2019, pp. 35–42. DOI: 10.5539/apr.v11n1p35

[6] Bhaskar, Sudhir, and Gupta, Sachin Kumar. "Bandwidth Improvement of Microstrip Patch Antenna Using H-Shaped Patch." International Journal of Engineering Research and Applications, vol. 2, no.1, pp. 1–5, 2012. ISSN: 2248-9622.

[7] Kumar, Alok, Nancy Gupta, and P. C. Gautam. "Gain and Bandwidth Enhancement Techniques in Microstrip Patch Antennas - A Review." International Journal of Computer Applications, vol. 148, no. 7, 2016, pp. 9–14. DOI: 10.5120/ijca2016911207.

[8] Yang, F., X. Zhang, X. Ye, and Y. Rahmat-Samii. "Wide-Band E-Shaped Patch Antennas for Wireless Communications." IEEE Transactions on Antennas and Propagation, vol. 49, no. 7, 2001, pp. 1094–1100. DOI: 10.1109/8.933489.

[9] Nandalal, V., Kumar, V. A., Sumalatha, M. S., & Manikandan, T. "Performance Evolution of Reconfigurable Antenna Using Contact and Non-Contact Feeding Technique." 2019 3rd

International Conference on Electronics, Communication and Aerospace Technology (ICECA),pp.954,June2019.DOI: 10.1109/ICECA.2019.8821933

[10] Paul, Liton Chandra, et al. "A Wideband Microstrip Patch Antenna with Slotted Ground Plane for 5G Application." Proceedings of the 2021 International Conference on Science & Contemporary Technologies (ICSCT), IEEE, 2021, pp. 1–5. DOI: 10.1109/ICSCT53883.2021.9642597.

[11] Tayyab, Umais, Kumar, Ashok, Petry, Hans-Peter, Asghar, Muhammad Ejaz, & Hein, Matthias A. "Dual-Band Nested Circularly Polarized Antenna Array for 5G Automotive Satellite Communications."Applied Sciences, vol. 13, no. 21, pp. 11915, 2023. DOI: [10.3390/app132111915](https://doi.org/10.3390/app132111915).

[12] Alalewi, Ahmad, Dayoub, Iyad, & Cherkaoui, Soumaya. "On 5G-V2X Use Cases and Enabling Technologies: A Comprehensive Survey." IEEE Access, vol. 9, pp. 107710–107737, 2021. DOI: 10.1109/ACCESS.2021.3100472

[13] Shimizu, Takayuki, Lu, Hongsheng, Kenney, John, & Nakamura, Shunsuke. "Comparison of DSRC and LTE-V2X PC5 Mode 4 Performance in High Vehicle Density Scenarios." Proceedings of the ITS World Congress, Singapore, pp. 1–7, October 2019.

[14] Abboud, Khaled, Omar, Hossam A., & Zhuang, Weihua. "Interworking of DSRC and Cellular Network Technologies for V2X Communications: A Survey." IEEE Transactions on Vehicular Technology, vol. 65, no. 12, pp. 9457–9470, Dec. 2016. DOI: 10.1109/TVT.2016.2591558.

[15] Kumar, Sachin, Lee, Gwan Hui, Kim, Dong Hwi, Haunan, Nashuha Syifa, Choi, Hyun Chul, & Kim, Kang Wook."Compact Planar Super-Wideband Monopole Antenna with Four Notched Bands."Electronics,vol.9,no.8,pp.1204,2020.DOI:[10.3390/electronics9081204]

[16] Tewary, Tapas, Maity, Souvik, Mukherjee, Sayantan, Roy, Abhijit, Sarkar, Pranabendu P., & Bhunia, Sudipta. "High Gain Miniaturized Super-Wideband Microstrip Patch Antenna." International Journal of Communication Systems, vol. 35, no. 11, pp. e5181, 2022. DOI: 10.1002/dac.5181.

[17] Sukri, Nur Afida, Faiza, Zafirah, Akhbar, Rabiatuladawiah, Azmin, Azwati, Ahmad Fauzi, Najwa Rawaida Ahmad, & Mozi, Aiza Mahyuni. "A Tri-Band Antenna for Satellite Applications at C, X and Ku Bands." 2021 IEEE Symposium on Wireless Technology & Applications(ISWTA),pp.11–15,2021.DOI: 10.1109/ISWTA52208.2021.9587392.

[18] Alibakhshi-Kenari, M., Naser-Moghadasi, M., Sadeghzadeh, R. A., Virdee, B. S., & Limiti, E. "A New Planar Broadband Antenna Based on Meandered Line Loops for Portable Wireless Communication Devices." Radio Science, vol. 51, no. 7, pp. 1109–1117, 2016. DOI: 10.1002/2016RS005973

[19] Alam, Md Mottahir, Azim, Rijal, Sobahi, Nawaf M., Khan, A. Iftikhar, & Islam, Mohammad Tariqul. "A Dual-Band CPW-Fed Miniature Planar Antenna for S-, C-, WiMAX, WLAN, UWB, and X-Band Applications." Scientific Reports, vol. 12, no. 1, p. 7584, 2022. DOI: https://doi.org/10.1038/s41598-022-11679-7

[20] Sifat, Rasheduzzaman, Faruque, Mohammad Rashed Iqbal, Hossain, Md Bellal, Abdullah, Mardina, Islam, Mohammad Tariqul, Khandaker, Mayeen Uddin, Tamam, Nissren, & Sulieman, Abdelmoneim."Development of Double C-Shaped Left-Handed Metamaterial for

Dual-Band Wi-Fi and Satellite Communication Application with High Effective Medium Ratio and Wide Bandwidth."Crystals, vol. 12, no. 6, p. 836, 2022. DOI: 10.3390/cryst12060836.

[21] Muzaffar, Sharjeel, Turab, Doha, Zahid, Muhammad, & Amin, Yasar. "Dual-Band UWB Monopole Antenna for IoT Applications." Engineering Proceedings, vol. 46, no. 1, p. 29, 2023. DOI:10.3390/engproc2023046029

[22] Naik, Gaurang, Biplav Choudhury, and Jung-Min Park, "IEEE 802.11bd 5G NR V2X: Evolution of radio access technologies for V2X communications," IEEE Access, vol. 7, pp. 70169–70 84, 2019. DOI: 10.1109/ACCESS.2019.2919489

[23] Li, Xiaoshuai, Lin Ma, Rajan Shankaran, Yubin Xu, and Mehmet A. Orgun, "Joint power control and resource allocation mode selection for safety-related V2X communication," IEEE Trans. Veh. Technol., vol. 68, no. 8,pp.970–7986,Aug.2019,DOI: 10.1109/TVT.2019.2921352

[24] Uddin, Md Nazim, Md Nurul Anwar Tarek, Md Khadimul Islam, and Elias A. Alwan "A Reconfigurable Beam steering Antenna Array at 28 GHz Using a Corporate-fed 3-Bit Phase Shifter". IEEE Open J. Antennas Propagation.2023,Vol.4, 126–140.DOI: 10.1109/OJAP.2023.3237882

[25] Saeed, Ahmed AA, Osama YA Saeed, Abdulguddoos SA Gaid, Amjad MH Aoun, and Amer A. Sallam. "A low Profile Multiband Microstrip Patch Antenna For 5G Mm-Wave Wireless Applications." In 2021 International Conference of Technology, Science and Administration (ICTSA), pp. 1-5. IEEE, 2021.DOI: 10.1109/ICTSA52017.2021.9406519

[26] Kulkarni, Jayshri. "Wideband cpw-fed oval-shaped monopole antenna for wi-fi5 and wi-fi6 applications." Progress In Electromagnetics Research C,vol.107, pp 173-182,2021, DOI:10.2529/2020EMC009354

[27] Hasan, Md Rabiul, Riheen, Md Ashraful, Sekhar, Pradipta, & Karacolak, Tayfun. "Compact CPW-Fed Circular Patch Flexible Antenna for Super-Wideband Applications." IET Microwaves, Antennas & Propagation, vol. 14, no. 10, pp. 1069–1073, Aug. 2020. DOI: 10.1049/iet-map.2020.0155.

[28] Kirtania, Sharadindu Gopal, Bachir Adham Younes, Abdul Rakib Hossain, Tutku Karacolak, and Praveen Kumar Sekhar. "CPW-Fed Flexible Ultra-Wideband Antenna for IoT Applications." Micromachines 12, no. 4 (2021): 453. DOI: 10.3390/mi12040453.

[29] Reddy, YV Bhaskar, A. Mallikarjuna Prasad, and K. Veera Swamy. "Wide Band Flexible Antenna For Future V2X And 5G Automotive Vehicular Imaging and Position Prediction Applications." International Journal of Intelligent Systems and Applications in Engineering 12.1 (2024): 689-695. ISSN:2147-67992

[30] Singh, Khushboo; Patil, Sonal; Naik, Ashwini; and Kadam, Sujata. "Hexagonal Microstrip Patch Antenna Design for UWB Application." ITM Web of Conferences, vol. 44, 2022, p. 02004. DOI: 10.1051/itmconf/20224402004.

[31] Mondal, Tapas; Samanta, Susamay; Ghatak, Rowdra; and Chaudhuri, Sekhar Ranjan Bhadra. "A Novel Tri-Band Hexagonal Microstrip Patch Antenna Using Modified Sierpinski Fractal for Vehicular Communication." Progress In Electromagnetics Research C, vol. 57, pp. 25–34, 2015. DOI: 10.2528/PIERC15021105.